OPTICA

Large circular dichroism in the emission from an incandescent metasurface

Anne Nguyen,[1] Jean-Paul Hugonin,[1] Anne-Lise Coutrot,[1] Enrique Garcia-Caurel,[2] Benjamin Vest,[1] and Jean-Jacques Greffet[1,*]

[1]Université Paris-Saclay, Institut d'Optique Graduate School, CNRS, Laboratoire Charles Fabry, 91127, Palaiseau, France
[2]LPICM, CNRS, Ecole polytechnique, Institut Polytechnique de Paris, Palaiseau, France
*Corresponding author: jean-jacques.greffet@institutoptique.fr

Received 4 November 2022; revised 27 December 2022; accepted 3 January 2023; published 30 January 2023

Compact sources in the mid-wave infrared (MWIR) are needed for applications ranging from spectroscopy to free-space communication. Ultrathin incandescent metasurfaces are promising candidates, offering the possibility to tune the emission spectrum, directivity, and modulation speed. However, control over polarization remains a challenge, especially when it comes to the emission of circularly polarized light. Here, we report the emission of polarized MWIR radiation from a 700 nm thick incandescent chiral metasurface. The degree of polarization is above 0.5 with degree of circular polarization of 0.38 at 5 μm. The metasurface is heated by the Joule effect, and the emission can be modulated beyond 10 MHz. This could enable detection techniques that use polarization as an additional degree of freedom.

https://doi.org/10.1364/OPTICA.480292

1. INTRODUCTION

Circularly polarized light (CPL) is uncommon in a natural environment. It was only recently discovered that few animal species are sensitive to visible CPL [1,2] and use it to send messages to other individuals of the same species. Such signals cannot be detected by predators that are usually insensitive to polarization, similarly to commercial IR detectors. Covert communication channels in the mid-wave infrared (MWIR) relying on circularly polarized (CP) signals can, therefore, be a direct application for security or military purposes. CPL in the IR is also useful for techniques such as vibrational circular dichroism (CD) spectroscopy [3] to determine the absolute configuration of small molecules. For all these applications, sources of CPL are needed. The generation of CPL is commonly done by using a source of unpolarized light followed by a linear polarizer and a quarter-wave plate optimized for the desired wavelength. However, such circular polarizers can hardly be integrated in a compact system. Linear polarizers in the MWIR can be made out of thin metallic wires, namely wire grid polarizers. They can also be directly integrated with a MWIR source offering the advantage of built-in polarization selective emission, hence improved energetic efficiency. For example, it has been demonstrated that incandescent subwavelength gratings of metallic wires can emit nearly 100% linearly polarized light [4]. In contrast, the retardation element generally relies on birefringent materials, liquid crystals, or total internal reflection such as in Fresnel rhombs and is, therefore, bulky. To obtain a retardance ϕ with a birefringent wave plate at wavelength λ between the slow and fast axes, a precise thickness $d = \lambda\phi/(2\pi\Delta n)$, Δn being the difference between the ordinary and extraordinary refractive indices, is needed. This bulkiness cannot be avoided unless a different paradigm is used. This is the goal of flat optics or metasurfaces, a field that has recently gained considerable interest for the miniaturization of optical elements. Many devices with differentiated CP responses based on subwavelength unit cells with structural chirality have been explored. Recent reviews [5–7] provide an overview of the state-of-the-art in terms of metamaterials and metasurfaces for polarization control.

Initial interest grew in CP selective filters. Using concepts developed in the framework of nanophotonics, 3D chiral photonic crystals have been considered as efficient CP-sensitive filters as they can have a photonic polarization-dependent stop band. Noticeable CD was theoretically predicted in arrays of helices standing in a dielectric background [8]. Experimental evidence was shown in transmission for dielectric [9] helices in the near-IR (NIR) or for metallic helices in the mid-IR [10], achieving up to 0.95 CD, and in reflection in the visible [11] with 0.64 peak CD. As fabrication procedures to build such continuous twisted structures are complex, a discretized alternative consisting of layers of dielectric woodpiles regularly twisted with respect to each other was proposed [12] and demonstrated experimentally [13] in the NIR. Stacks of arrays of twisted split ring resonators [14] have been demonstrated in the MWIR. Experiments in the visible [15] with twisted photonic crystals using a number of layers on the order of 10 have also been reported. However, for enhanced compactness and minimal fabrication steps, chiral planar metasurfaces are highly desirable.

Such metasurfaces were first reported in [16] where linear-to-circular polarization conversion in reflection occurs on the 2D metallic array of gammadions with an opposite ellipticity of light

depending on the orientation of the gammadions. Polarization converters were also proposed [17] using a meanderline metallic metasurface as a broadband polarization converter in reflection in the long-wave infrared (LWIR) to obtain CP light from a linearly polarized impinging beam. Dielectric metasurfaces have also been used for polarization conversion in transmission [18].

Interest also emerged for chiral metasurfaces to build CP-sensitive detectors. The authors of [19] proposed an Archimedean spiral composed of thermocouples as a CP-sensitive detector in the LWIR. Local absorption occurs at different locations, resulting in temperature differences that induce a different voltage. Plasmonic zigzag-shaped metamaterials can also behave as CP selective absorbers [20–22]. The authors of [20,22] obtained similar levels of dichroism with a 0.7 peak contrast in absorption in the NIR.

As for CP emission, seldom solutions have been proposed up to now. It has been suggested [23] that spontaneous emission could not produce CPL due to the fact that random thermal current densities along two axes are uncorrelated according to fluctuation-dissipation theorem for an isotropic medium. As a consequence, they could not generate polarized fields. While this is the case for emission in a homogeneous and isotropic medium, when emission is mediated by a resonator or cavity, the emission process is different. Fluctuating current densities excite the resonator or cavity modes generating induced current densities that then radiate. These induced current densities can radiate CP fields. A well-known example illustrating the difference between fluctuating currents and induced currents is thermal emission by a grating supporting surface phonon polaritons [24]. The induced currents generate a directional emission. Similarly, polarized emission may occur when designing surface sustaining modes with appropriate correlations of the induced current densities components.

These ideas have been implemented a few times in the visible and NIR range. Quantum dots embedded in the middle of a chiral 3D photonic crystal [25,26] show a degree of circular polarization (DOCP) up to 0.5. A variant with quantum dots lying beneath arrays of planar gammadions [27] shows a DOCP of 0.2 at best.

The field of incandescent sources of CP radiation is still in its infancy. A procedure to design thermal metasurfaces with a large degree of polarization (DOP) has been proposed [28] but not yet implemented experimentally. To the best of our knowledge, circular emission was first reported using metasurfaces based on geometric phase engineering allowing spin–orbit interaction [29]. This proof of principle did not report quantitative characterization. A qualitative result was also reported in [30] using an array of tripods. Generation of circular polarization was reported by shaping unpolarized emission by a blackbody emitter using wire grid polarizers to generate linearly polarized LWIR radiation followed by a linear-to-circular polarization converter [23,30]. The device achieves a 0.28 DOCP with a total DOP of 0.84. Although these sources are less than 1.5 μm thick, they still need an intermediate step for polarization conversion, which leads to a reduced device efficiency. A recent preprint reports a thermal metasurface producing a DOCP of 0.4 [31]. In summary, while there are many reports demonstrating thermal metasurfaces controlling the emission spectrum, direction of emission and linear polarization, the emission of pure CP thermal radiation by a metasurface is still a challenge.

In this paper, we introduce an incandescent metasurface optimized for the MWIR that emits CPL with a DOP larger than 0.5 on a large spectral range from 5 to 7 μm. A large CD of 0.38 is reached at 5 μm. To analyze theoretically the origin of the CD, we study the quasi-normal modes (QNMs) of the structure and find a large difference in their coupling to each helicity of circular polarization. In contrast with sources that have been reported in the literature for CP emission, we use a compact metasurface (25 nm thick), which can be heated electrically and modulated up to 10 MHz. To our knowledge, no equivalent thin metasurface with a controlled polarization state has been published up to now.

2. RESULTS

A. Design of the Device

We envision a metallic metasurface spectrally optimized to emit in the MWIR with a large DOP where CD is dominant. Control over the spectral range of emission can be done by engineering the emissivity spectrum of the metasurface. To do this, we rely on Kirchhoff's law establishing the equality between emissivity and absorptivity [32]. To control the absorptivity spectrum, we use a Salisbury screen configuration, where an absorbing thin metallic film is deposited above a mirror at a well-chosen distance. Constructive interference between the incoming and reflected wave result in a stationary wave in the medium. We can, thus, reach a 100% absorption level at the desired wavelength by placing the metallic film at an antinode of this stationary wave [33]. Local Kirchhoff's law [34] guarantees that, when heated, the same metallic film will achieve an emissivity peak close to 1. This configuration enables us to easily tune the emission peak wavelength.

Such a structure emits unpolarized light. To design a source that emits CPL in the normal direction, we design a metasurface with a preferential coupling to one helicity in the far-field. We texture the thin film and shape arrays of Z-shaped or half-gammadion resonators to form a chiral unit cell (see Fig. 1). We designed the device to obtain large CD in the MWIR at 4.7 μm.

In a Salisbury configuration, the emission is due to thermally induced current density fluctuations in the metallic wires. Hence, it is sufficient to heat the metasurface while leaving the substrate cold. Since the system is not isothermal, Kirchhoff's law cannot be directly used. To design the source, we make use of the local Kirchhoff's law [34], which can be used for objects with arbitrary shape and temperature field, provided that local thermodynamic equilibrium is reached. To ensure local heating, we connect the individual Z-shaped resonators to their neighbors forming nanowires as seen in Fig. 1. We deposit electrical contacts on both ends of the structure. This connected architecture can be heated locally through the Joule effect by applying a voltage. Besides, as discussed in [4], this configuration enables modulation of the emitted light beyond 10 MHz, 5 orders of magnitude faster than commercially available incandescent sources. As the structure consists of successive constrictions, the temperature increase is expected to be inhomogeneous with maxima around the constrictions. Platinum is chosen for the nanowires as it can sustain high temperatures and has a good adhesion on silicon nitride (SiN_x) [35]. We use SiN_x as the transparent spacer in the MWIR and an optically thick layer of molybdenum as the mirror, which is compatible with SiN_x. The sample was fabricated using electronic lithography as detailed in Supplement 1.

Rigorous coupled-wave analysis (RCWA) calculations yielding the total absorption spectrum and absorption occurring exclusively inside the platinum metasurface are shown in Fig. 2(a). It is seen

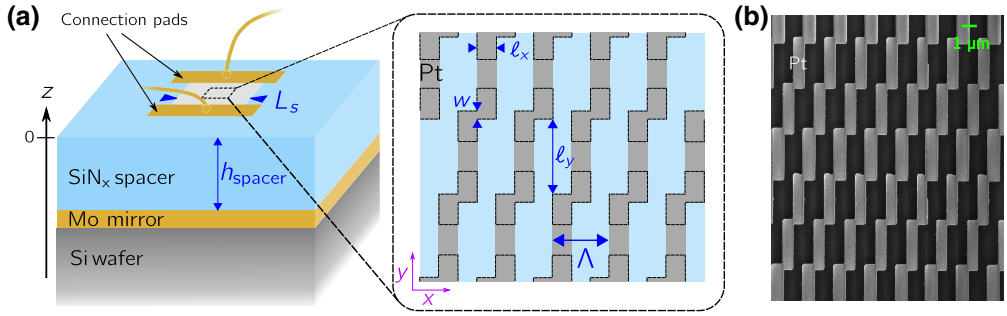

Fig. 1. (a) Schematic view of the device. $\ell_x = 688$ nm, $\ell_y = 2.737$ µm, $w = 300$ nm, $\Lambda = 2.063$ µm, $h_{spacer} = 651$ nm, $h_{Pt} = 25$ nm. Dotted lines on the platinum structure serve as visual guides to mark out the Z-shaped pattern; they have no physical existence. The metasurface is $L_s \times L_s = 100 \times 100$ µm^2 large. (b) SEM picture of the fabricated device. Scale bar, 1 µm.

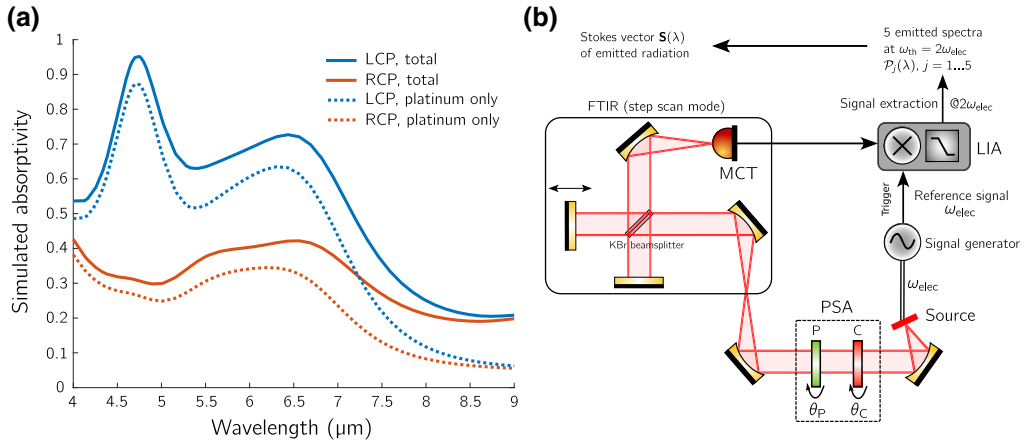

Fig. 2. (a) Simulated absorption spectrum under a circularly polarized plane wave under normal incidence. Thick lines represent total absorption, and dotted lines stand for absorption in the platinum structure only. (b) Stokes vector characterization setup. The device is positioned in the focal plane of a collection mirror to produce a collimated beam entering the polarization state analyzer (PSA). The intensity is focused into the input slit of a FTIR. The intensity is then collected by a MCT detector. The spectrum at frequency ω_{th} is extracted with a lock-in amplifier. The operation is repeated for each of the five polarization projection states of the PSA.

that absorption essentially takes place in the platinum, as expected for a Salisbury architecture.

B. Operating the Source

In order to heat the metallic wires, we apply a sinusoidal voltage on the device with an amplitude of 13 V peak-to-peak and oscillating at frequency $\omega_{elec}/(2\pi)$. The temperature of the platinum evolves in time as $T(\mathbf{r}, t) = T_0 + T_{DC}(\mathbf{r}) + T_{AC}(\mathbf{r}, \omega_{th})\cos(\omega_{th} t)$ with $\omega_{th} = 2\omega_{elec}$. Since the electrical resistance of platinum varies linearly with temperature, measuring the current passing through the metasurface yields its electrical resistance and, hence, the spatially averaged temperature. We find $T_{DC} \simeq 180°C$ and $T_{AC} \simeq 118°C$ when using $\omega_{elec}/(2\pi) = 10$ kHz. Assuming that emission essentially comes from the platinum metasurface at $z = 0$, the power emitted at frequency ω_{th} in a solid angle $d\Omega$ in the normal direction $\mathbf{e}_z$ can be cast in the following form [4]:

$$P_e(\lambda, \omega_{th}, \mathbf{e}_z) \simeq d\Omega \frac{L_s^2}{2} \frac{\partial I_{BB}}{\partial T}[\lambda, T_0 + T_{DC}(z=0)] \times \left[A^{(LCP)}(\lambda, -\mathbf{e}_z) + A^{(RCP)}(\lambda, -\mathbf{e}_z)\right] \bar{T}_{AC}(\omega_{th}), \quad (1)$$

where I_{BB} is the blackbody radiance, $A^{(\ell)}(\lambda, \mathbf{e}_z)$ is the absorptivity under normal incidence for a circular polarization $\ell =$ (LCP, RCP), and L_s is the size of the square platinum metasurface. $\bar{T}_{AC}(\omega_{th})$ is the oscillation amplitude of the temperature increase at frequency ω_{th} in the platinum, averaged over the overall platinum volume. More details on the derivation of this equation can be found in Supplement 1. The emitted light passes through a polarization state analyzer (PSA) and is measured by the spectrometer in the step scan mode. The measured output is, thus, proportional to $\mathcal{R}(\lambda)\mathcal{P}(\lambda)\partial I_{BB}/\partial T[\lambda, T_0 + T_{DC}(z_0)]\bar{T}_{AC}(\omega_{th})$, where $\mathcal{R}(\lambda)$ is the spectral response of the detector and $\mathcal{P}(\lambda)$ encompasses information on the polarization state selected by the PSA.

C. High Frequency Modulation of the Incandescent Source

In this section, we show that the amplitude of the emitted power can be modulated beyond 10 MHz. To characterize the source dynamic response, we modulate its temperature by applying an oscillating voltage on the electrically connected chiral platinum nanowires. The experimental setup is similar to the one described in [4]. We use a lock-in amplifier to extract the amplitude of the emitted intensity. Results are shown in Fig. 3. Two regimes can be observed as a function of the modulation frequency. In the low-frequency regime (blue shade) below 10^5 Hz, the signal amplitude is almost constant. In the high-frequency regime (pink shade), the

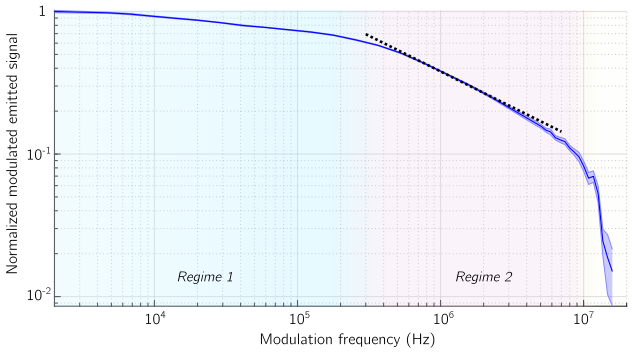

Fig. 3. Measured frequency response of the source normalized to the modulated intensity emitted at 2 kHz. The modulation frequency is $f_{\text{th}} = 2 f_{\text{elec}}$. Error bars represent $1-\sigma$ error bars. The black dotted line indicates a $1/\sqrt{f_{\text{th}}}$ behavior fitted on the experimental data. The pink shaded area corresponds to this frequency regime, whereas the blue shaded area corresponds to a constant frequency regime.

signal decays as $1/\sqrt{\omega_{\text{th}}}$. These two regimes are dictated by the temperature dynamics of the system as discussed in [4,36]. The signal falloff above 10 MHz is due to the detector frequency cutoff.

D. Polarimetric Characterization

The polarization state of partially polarized light is best described by its Stokes vector $\mathbf{S}(\lambda) = [S_0(\lambda), S_1(\lambda), S_2(\lambda), S_3(\lambda)]$, whose components are defined as $S_0 = \langle |E_x|^2 + |E_y|^2 \rangle$, $S_1 = \langle |E_x|^2 - |E_y|^2 \rangle$, $S_2 = 2\text{Re}\langle (E_x E_y^*) \rangle$, and $S_3 = -2\text{Im}\langle (E_x E_y^*) \rangle$, where the brackets denote statistical average. E_x and E_y denote the projection of the electric field along the x and y axes represented in Fig. 1. The Stokes parameters contain information on the correlation between orthogonal components of the electric field and can be measured by performing intensity measurements. In particular, S_0 is proportional to the time averaged z-component of the Poynting vector $I_{\text{tot}} = \epsilon_0 c\, S_0/2$. $S_1 = I_x - I_y$ and $S_2 = I_{45°} - I_{-45°}$ are the difference of intensities corresponding to fields polarized along the x and y directions, along two axes rotated by 45° and −45° with respect to the x axis, respectively, and $S_3 = I_{\text{RCP}} - I_{\text{LCP}}$ is the difference of intensity between the right-handed circular polarization (RCP) and left-handed circular polarization (LCP) components. These measurements are easily done for one wavelength with a polarizer and a quarter-wave plate. In practice, the retarder behaves as a quarter-wave plate only for a given wavelength. When working at other wavelengths, the retardance differs, and analysis of circular polarization states is no longer straightforward. Still, the Stokes vector can be retrieved provided that the Mueller matrix of the wave plate is fully characterized and for wavelengths such that the wave plate does not behave as a $n\pi$ retarder. The general procedure developed to extract the Stokes vector from a set of five independent measurements is briefly described in Supplement 1.

With this method, the Stokes vector can be recovered over a spectral range spanning from 3.5 μm to 8 μm. Figure 4 shows the measured Stokes vector of the emitted light normalized by the total intensity as a function of wavelength. The corresponding DOP is plotted in Fig. 5.

The experimental observations can be compared to simulations. Absorption of a plane wave under normal incidence with linear

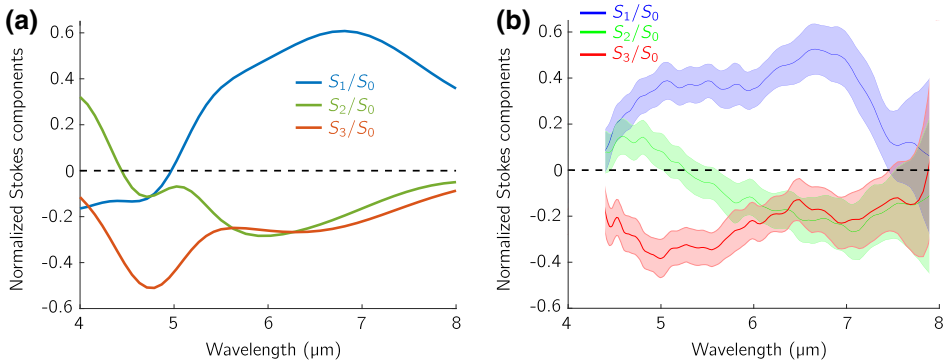

Fig. 4. Calculated (left) and experimentally measured (right) normalized Stokes parameters of the metasurface emission. The S_3 component is reversed in the simulation to allow comparison with the experimental results. Discontinuity around 4.2 μm in the experimental plot accounts for the CO_2 absorption line. Shaded areas represent $1-\sigma$ error bars.

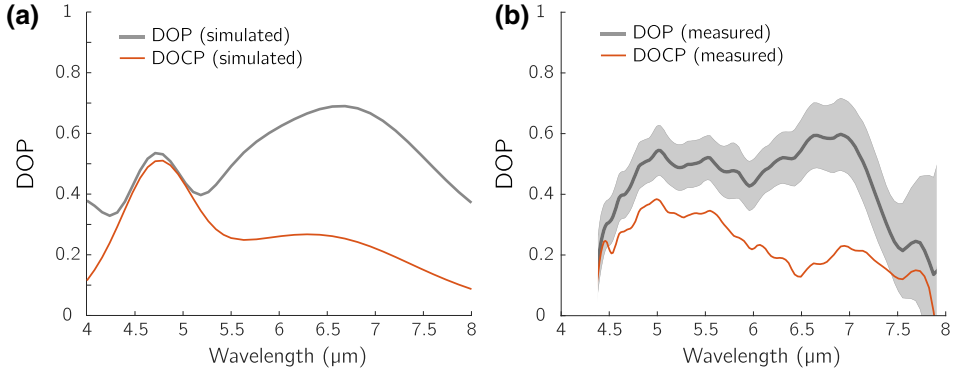

Fig. 5. (a) Simulated and (b) measured degree of polarization (DOP) and degree of circular polarization (DOCP). Shaded areas represent one-sigma error bars.

and circular polarizations is computed to obtain $S_0 = A_x + A_y$, $S_1 = A_x - A_y$, $S_2 = A_{45°} - A_{-45°}$, and $S_3 = -(A_{\mathrm{RCP}} - A_{\mathrm{LCP}})$, where A_v is the absorption of a v-polarized plane wave under normal incidence. Note the minus sign affecting the S_3 component due to the inversion of helicity of light, which depends on the direction of propagation and is, therefore, reversed between emission and absorption.

Experimental results are in fair agreement with the simulations. As seen in Fig. 4(a), the surface was designed to present a peak in S_3 at 4.7 μm. We indeed observe a peak in S_3 of −0.4 at 5 μm. From the knowledge of the Stokes vector, we can extract the DOP $= \sqrt{S_1^2 + S_2^2 + S_3^2}/S_0$ of the source as well as its DOCP $= |S_3/S_0|$, as shown in Fig. 5. We have, therefore, characterized the incandescent source as emitting above 40% of polarized radiation with an elliptic polarization on a spectral range extending from 4.6 μm to 7.2 μm, with a maximum reaching 60%. Although the polarized part of the emission is predicted to be close to purely circular at 4.7 μm, experimental characterization shows an additional linear dichroism in the 4.5–5.5 μm range. All these results are analyzed in the next section.

3. DISCUSSION

A. Absorption Mapping Depending on Polarization

To investigate the origin of the large DOCP around 5 μm, we start by comparing the mapping of the local absorption in the platinum structure when it is illuminated by a left or right circular polarization. Figure 6(a) shows a map of the local absorption inside the platinum for each polarization at $\lambda_0 = 4.7$ μm. Absorption is much larger for left circular polarization and occurs mainly in the constrictions. From the local Kirchhoff's law, it follows that LCP radiation is emitted mostly by the constrictions confirming that the z-shaped structure plays an important role.

B. Modal Description

To have a better understanding of the origin of the absorption contrast depending on the polarization of the incident plane wave, we investigate the modes of the chiral metasurface. An appropriate theoretical tool for such open and lossy systems is the QNM formalism. Most generally, the electromagnetic fields can be written as

$$\boldsymbol{\Psi}^{(\ell)}(\mathbf{r}, \omega) = \boldsymbol{\Psi}_{\boldsymbol{b}}^{(\ell)}(\mathbf{r}, \omega) + \boldsymbol{\Psi}_{\boldsymbol{s}}^{(\ell)}(\mathbf{r}, \omega), \tag{2}$$

where (ℓ) stands for the polarization, $\boldsymbol{\Psi} = [\mathbf{E}, \mathbf{H}]$ is the total field, and $\boldsymbol{\Psi}_{\boldsymbol{b}} = [\mathbf{E}_b, \mathbf{H}_b]$ is the background field satisfying source-free Maxwell equations in the absence of the perturbation, i.e., the

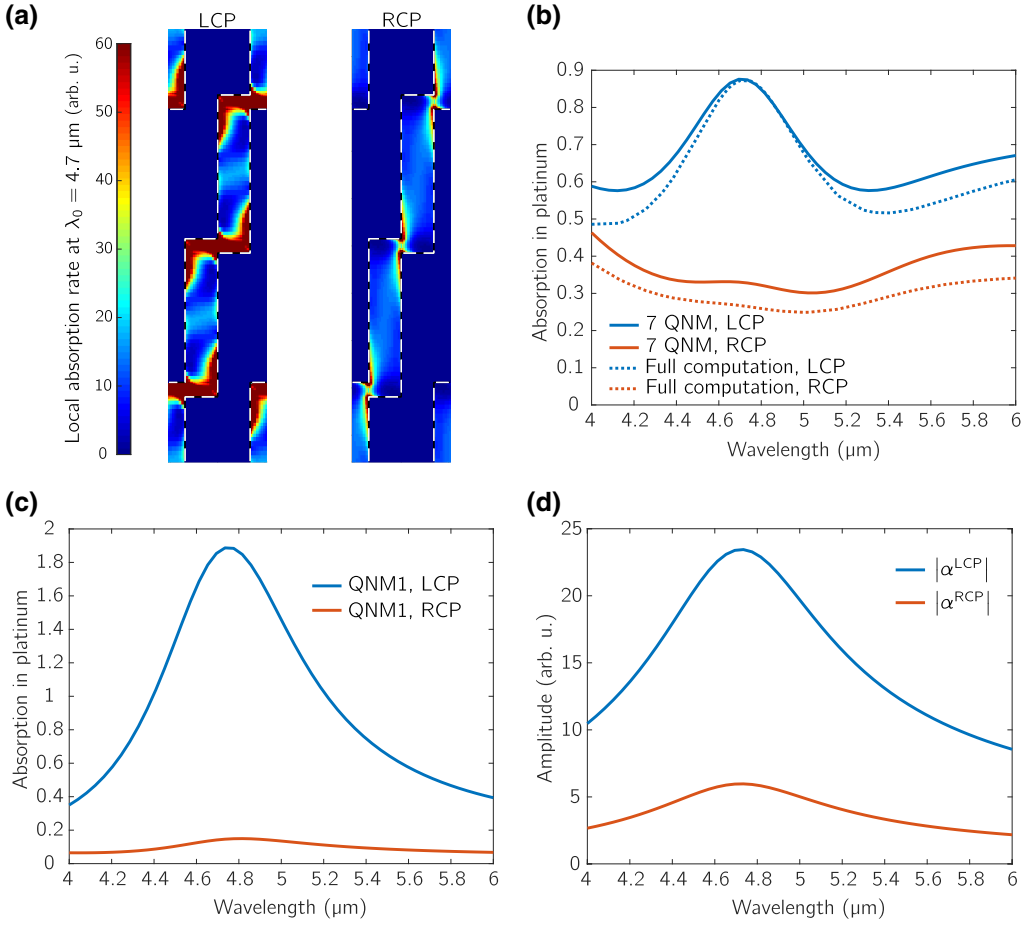

Fig. 6. (a) Local absorption rate $\pi/\lambda_0\sqrt{\epsilon_0/\mu_0}\mathrm{Im}[\epsilon(\mathbf{r}, \lambda_0)]|\mathbf{E}^{(\ell)}(\mathbf{r}, \lambda_0)|^2$ of a LCP/RCP plane wave under normal incidence at $\lambda_0 = 4.7$ μm. The colormap is identical for both polarizations. (b) Simulated absorption in platinum illuminated by an LCP/RCP polarized plane wave as the field is truncated to 7 QNMs. (c) Simulated absorption in platinum illuminated by an LCP/RCP polarized plane wave as the field is truncated to QNM1 only. Due to the truncation, i.e., the absence of interference between QNMs, absorption may be larger than 1. (d) Norm of the LCP/RCP excitation coefficients for QNM1.

permittivity at the location of the resonators is replaced by the permittivity in the medium surrounding the perturbation $\varepsilon_b(\omega)$. $\mathbf{\Psi}_s = [\mathbf{E}_s, \mathbf{H}_s]$ is the field scattered by the perturbation that has a permittivity $\Delta\varepsilon(\omega)$. The scattered electromagnetic fields can be expanded as [37]

$$\mathbf{\Psi}_s^{(\ell)}(\mathbf{r}, \omega) \simeq \sum_{m=1}^{M} \alpha_m^{(\ell)}(\omega)\hat{\mathbf{\Psi}}_m(\mathbf{r}), \tag{3}$$

where $\hat{\mathbf{\Psi}}_m = [\hat{\mathbf{E}}_m, \hat{\mathbf{H}}_m]$ is a normalized QNM corresponding to pole $\tilde{\omega}_m$ of the scattering matrix, $\alpha_m^{(\ell)}(\omega)$ is the polarized complex excitation coefficient weighting the contribution of the QNM labeled m and solely depends of the frequency, and M is the minimum number of QNMs needed to reach convergence.

To grasp the physics taking place around 5 μm leading to the CD, we look for the dominant QNM in this spectral range and consider their weight in the scattered fields. The excitation coefficient can be written as [38]

$$\alpha_m^{(\ell)}(\omega) = \frac{\omega}{\tilde{\omega}_m - \omega} \int_V \Delta\varepsilon(\mathbf{r}, \omega)\mathbf{E}_b^{(\ell)}(\mathbf{r}, \omega) \cdot \hat{\mathbf{E}}_m(\mathbf{r})\mathrm{d}^3\mathbf{r}, \tag{4}$$

where V is the geometric volume of the perturbation. Equation (4) is valid provided that the so-called normalization condition is fulfilled. Normalization of the QNM is done here according to the procedure proposed by [37]. Numerical simulations of our system were performed in two main steps. First, the metasurface was reduced to a homogeneous platinum layer with same thickness of 25 nm, i.e., the unperturbed configuration is a simple Salisbury screen, and the corresponding background field is computed. Then, the resonant structures were added as a perturbation. In our case, airholes drilled through the homogeneous platinum so as to recover the metasurface in Fig. 1(b). When excited by the background field, these perturbations give rise to a scattered field $\mathbf{\Psi}_S$. Volume V for the integration in Eq. (4) is, thus, the volume of the airholes in the metasurface. Further details on the normalization of the QNM and the derivation of the excitation coefficients can be found in Supplement 1.

A precise reconstruction of the absorption spectrum would require considering several QNMs and static modes as well [39] to guarantee energy conservation. However, a good approximation is obtained for seven QNMs, as shown in Fig. 6(b). Among the identified QNMs, the mode labeled QNM1 (see Fig. S1 in Supplement 1) is dominant and responsible for the CD around 4.7 μm. Figure 6(c) represents the absorption spectrum in the metallic resonators when using this single QNM. It is seen that the spectral dependence of the contribution of QNM1 accounts for most of the circular polarization absorption. Hence, we attribute the generation of CD to the thermal excitation of this particular QNM. In spite of absorption exceeding unity, it is informative to see that this single QNM induces a large CD by itself. Figure 6(d) shows the norm of the LCP and RCP excitation coefficient of QNM1. Around 4.7 μm, the RCP coupling amplitude is nearly 5 times larger than the LCP coupling, which is at the origin of the CD. QNM1 is, therefore, better coupled to one circular polarization in the normal direction compared to the cross polarization.

A second QNM, labeled QNM2, has been identified. The corresponding pole lies close to QNM1. In contrast with QNM1, QNM2 shows a strong linear dichroism (see Supplement 1 for further discussion). Deviation to theory in the [4.5–5.5] μm range, as seen in Fig. 4, is attributed to a spectral shift of the poles caused by fabrication defects of the platinum structure.

4. CONCLUSION

In summary, we have built a submicrometer thick source based on a chiral metasurface. Upon heating, it emits elliptically polarized light over a broad spectral range. The emission has a high DOP reaching up to 0.54 at 5 μm, with a DOCP as high as 0.38. The design of the source relies on chiral sub-units that have modes coupling efficiently to one circular polarization and poorly to the other. Optimization of the source requires a control over its polarized emissivity as well as over the distribution of temperature elevation throughout the structure. Thanks to the source architecture, modulation up to 10 MHz of the emission can be achieved through temperature modulation of the source, relying on heat conduction to a colder underlying substrate. The device presented in this work enables us to control the polarization and spectrum of the emitted radiation indicating that incandescent metasurfaces offer a versatile platform for MWIR emission.

Funding. Agence Nationale de la Recherche (ANR-17-CE24-016).

Acknowledgment. A. N. acknowledges support from Direction Générale de l'Armement. Author contributions: J.-J. G. proposed and supervised the project. A. N. designed and fabricated the device. A.-L. C. participated in the device fabrication. A. N. performed the numerical simulations. J.-P. H. participated in the numerical simulations. A. N. and E. G.-C. designed the experimental setup. E. G.-C. and B. V. advised on the choice of polarization optical elements. A. N. performed the device characterization and analyzed the data. A. N. and J.-J. G. wrote the paper with input from all authors.

Disclosures. The authors declare no conflicts of interest.

Data availability. Raw experimental data and corresponding processing scripts can be found in the repository in [40].

Supplemental document. See Supplement 1 for supporting content.

REFERENCES

1. T.-H. Chiou, S. Kleinlogel, T. Cronin, R. Caldwell, B. Loeffler, A. Siddiqi, A. Goldizen, and J. Marshall, "Circular polarization vision in a stomatopod crustacean," Curr. Biol. **18**, 429–434 (2008).
2. Y. Gagnon, R. Templin, M. How, and N. Marshall, "Circularly polarized light as a communication signal in mantis shrimps," Curr. Biol. **25**, 3074–3078 (2015).
3. L. A. Nafie, "Vibrational circular dichroism: a new tool for the solution-state determination of the structure and absolute configuration of chiral natural product molecules," Nat. Prod. Commun. **3**, 1934578X0800300 (2008).
4. L. Wojszvzyk, A. Nguyen, A.-L. Coutrot, C. Zhang, B. Vest, and J.-J. Greffet, "An incandescent metasurface for quasimonochromatic polarized mid-wave infrared emission modulated beyond 10 MHz," Nat. Commun. **12**, 1492 (2021).
5. Y. Luo, C. Chi, M. Jiang, R. Li, S. Zu, Y. Li, and Z. Fang, "Plasmonic chiral nanostructures: chiroptical effects and applications," Adv. Opt. Mater. **5**, 1700040 (2017).
6. J. T. Collins, C. Kuppe, D. C. Hooper, C. Sibilia, M. Centini, and V. K. Valev, "Chirality and chiroptical effects in metal nanostructures: fundamentals and current trends," Adv. Opt. Mater. **5**, 1700182 (2017).
7. W. Li and S. Fan, "Nanophotonic control of thermal radiation for energy applications," Opt. Express **26**, 15995–16021 (2018).
8. A. Chutinan and S. Noda, "Spiral three-dimensional photonic-band-gap structure," Phys. Rev. B **57**, R2006–R2008 (1998).
9. M. Thiel, M. Decker, M. Deubel, M. Wegener, S. Linden, and G. von Freymann, "Polarization stop bands in chiral polymeric three-dimensional photonic crystals," Adv. Mater. **19**, 207–210 (2007).

10. J. K. Gansel, M. Thiel, M. S. Rill, M. Decker, K. Bade, V. Saile, G. V. Freymann, S. Linden, and M. Wegener, "Gold helix photonic metamaterial as broadband circular polarizer," Science **325**, 1513–1515 (2009).
11. M. Rajaei, J. Zeng, M. Albooyeh, M. Kamandi, M. Hanifeh, F. Capolino, and H. K. Wickramasinghe, "Giant circular dichroism at visible frequencies enabled by plasmonic ramp-shaped nanostructures," ACS Photon. **6**, 924–931 (2019).
12. J. C. W. Lee and C. T. Chan, "Circularly polarized thermal radiation from layer-by-layer photonic crystal structures," Appl. Phys. Lett. **90**, 051912 (2007).
13. M. Thiel, G. V. Freymann, and M. Wegener, "Layer-by-layer three-dimensional chiral photonic crystals," Opt. Lett. **32**, 2547–2549 (2007).
14. M. Decker, R. Zhao, C. M. Soukoulis, S. Linden, and M. Wegener, "Twisted split-ring-resonator photonic metamaterial with huge optical activity," Opt. Lett. **35**, 1593–1595 (2010).
15. Y. Zhao, M. A. Belkin, and A. Alù, "Twisted optical metamaterials for planarized ultrathin broadband circular polarizers," Nat. Commun. **3**, 870 (2012).
16. A. Papakostas, A. Potts, D. M. Bagnall, S. L. Prosvirnin, H. J. Coles, and N. I. Zheludev, "Optical manifestations of planar chirality," Phys. Rev. Lett. **90**, 107404 (2003).
17. S. L. Wadsworth and G. D. Boreman, "Broadband infrared meanderline reflective quarter-wave plate," Opt. Express **19**, 10604–10612 (2011).
18. C. Wu, N. Arju, G. Kelp, J. A. Fan, J. Dominguez, E. Gonzales, E. Tutuc, I. Brener, and G. Shvets, "Spectrally selective chiral silicon metasurfaces based on infrared Fano resonances," Nat. Commun. **5**, 3892 (2014).
19. E. Briones, A. Cuadrado, J. Briones, R. D. D. León, J. C. Martínez-Antón, S. McMurtry, M. Hehn, F. Montaigne, J. Alda, and F. J. González, "Seebeck nanoantennas for the detection and characterization of infrared radiation," Opt. Express **22**, A1538–A1546 (2014).
20. W. Li, Z. J. Coppens, L. V. Besteiro, W. Wang, A. O. Govorov, and J. Valentine, "Circularly polarized light detection with hot electrons in chiral plasmonic metamaterials," Nat. Commun. **6**, 8379 (2015).
21. W. Liu, L. Mei, Y. Li, L. Yu, Z. Lai, T. Yu, and H. Chen, "Controlling the spin-selective absorption with two-dimensional chiral plasmonic gratings," Opt. Lett. **44**, 5868–5871 (2019).
22. L. Ouyang, W. Wang, D. Rosenmann, D. A. Czaplewski, J. Gao, and X. Yang, "Near-infrared chiral plasmonic metasurface absorbers," Opt. Express **26**, 31484–31489 (2018).
23. S. L. Wadsworth, P. G. Clem, E. D. Branson, and G. D. Boreman, "Broadband circularly-polarized infrared emission from multilayer metamaterials," Opt. Mater. Express **1**, 466–479 (2011).
24. J.-J. Greffet, R. Carminati, K. Joulain, J.-P. Mulet, S. Mainguy, and Y. Chen, "Coherent emission of light by thermal sources," Nature **416**, 61–64 (2002).
25. S. Takahashi, Y. Ota, T. Tajiri, J. Tatebayashi, S. Iwamoto, and Y. Arakawa, "Circularly polarized vacuum field in three-dimensional chiral photonic crystals probed by quantum dot emission," Phys. Rev. B **96**, 195404 (2017).
26. A. A. Maksimov, I. I. Tartakovskii, E. V. Filatov, S. V. Lobanov, N. A. Gippius, S. G. Tikhodeev, C. Schneider, M. Kamp, S. Maier, S. Höfling, and V. D. Kulakovskii, "Circularly polarized light emission from chiral spatially-structured planar semiconductor microcavities," Phys. Rev. B **89**, 045316 (2014).
27. K. Konishi, M. Nomura, N. Kumagai, S. Iwamoto, Y. Arakawa, and M. Kuwata-Gonokami, "Circularly polarized light emission from semiconductor planar chiral nanostructures," Phys. Rev. Lett. **106**, 057402 (2011).
28. A. C. Overvig, S. A. Mann, and A. Alù, "Thermal metasurfaces: complete emission control by combining local and nonlocal light-matter interactions," Phys. Rev. X **11**, 021050 (2021).
29. N. Dahan, Y. Gorodetski, K. Frischwasser, V. Kleiner, and E. Hasman, "Geometric doppler effect: spin-split dispersion of thermal radiation," Phys. Rev. Lett. **105**, 136402 (2010).
30. J. Ginn, D. Shelton, P. Krenz, B. Lail, and G. Boreman, "Polarized infrared emission using frequency selective surfaces," Opt. Express **18**, 4557–4563 (2010).
31. X. Wang, T. Sentz, S. Bharadwaj, S. Ray, Y. Wang, D. Jiao, L. Qi, and Z. Jacob, "Observation of non-vanishing optical helicity in thermal radiation from symmetry-broken metasurfaces," arXiv, arXiv:2205.05926 (2022).
32. G. Kirchhoff, "On the relation between the radiating and absorbing powers of different bodies for light and heat," London Edinburgh Dublin Philos. Mag. J. Sci. **20**, 1–21 (1860).
33. S. Bauer, "Optical properties of a metal film and its application as an infrared absorber and as a beam splitter," Am. J. Phys. **60**, 257–261 (1992).
34. J.-J. Greffet, P. Bouchon, G. Brucoli, and F. Marquier, "Light emission by nonequilibrium bodies: local Kirchhoff law," Phys. Rev. X **8**, 021008 (2018).
35. P. Barritault, M. Brun, S. Gidon, and S. Nicoletti, "Mid-IR source based on a free-standing microhotplate for autonomous CO_2 sensing in indoor applications," Sens. Actuators A **172**, 379–385 (2011).
36. A. Nguyen and J.-J. Greffet, "Efficiency optimization of mid-infrared incandescent sources with time-varying temperature," Opt. Mater. Express **12**, 225–239 (2022).
37. Q. Bai, M. Perrin, C. Sauvan, J.-P. Hugonin, and P. Lalanne, "Efficient and intuitive method for the analysis of light scattering by a resonant nanostructure," Opt. Express **21**, 27371–27382 (2013).
38. P. Lalanne, W. Yan, K. Vynck, C. Sauvan, and J.-P. Hugonin, "Light interaction with photonic and plasmonic resonances," Laser Photon. Rev. **12**, 1700113 (2018).
39. C. Sauvan, "Quasinormal modes expansions for nanoresonators made of absorbing dielectric materials: study of the role of static modes," Opt. Express **29**, 8268–8282 (2021).
40. A. Nguyen, J.-P. Hugonin, A.-L. Coutrot, E. Garcia-Caurel, B. Vest, and J.-J. Greffet, "Large circular dichroism in the emission from an incandescent metasurface [Data set]," Zenodo (2023) https://doi.org/10.5281/zenodo.7538698.